Journal of Petroleum Science and Engineering 205 (2021) 108882

Contents lists available at ScienceDirect

Journal of Petroleum Science and Engineering

journal homepage: www.elsevier.com/locate/petrol

Rock mechanics and wellbore stability of deep shale during drilling and completion processes

Houbin Liu [a], Shuai Cui [a,**], Yingfeng Meng [a,*], Ze Li [a], Xingchuan Yu [a], Hangrui Sun [a], Yanxing Zhou [b], Yi Luo [c]

[a] State Key Laboratory of Oil and Gas Reservoir Geology and Exploitation, Southwest Petroleum University, Chengdu, 610500, China
[b] Department of Security and Fire Protection, Southwest Petroleum University, Chengdu, 610500, Sichuan, China
[c] Communication and Information Technology Center of Petrochina Company Limited, Southwest Oil & Gas Field Branch, Suining, 629000, Sichuan, China

ARTICLE INFO

Keywords:
Deep shale
Wellbore stability
Drilling and completion
Seepage field
Stress field
Collapse pressure

ABSTRACT

The seepage coupling effect between the borehole rock mass and borehole fluid and the effective stress field distribution around the wellbore are obviously different under different working conditions of drilling, fracturing and completion, which affect the stability of horizontal borehole of shale gas reservoir. The physical, chemical, and mechanical properties of the shale in Longmaxi formations in a block of China immersed with different working fluids were tested experimentally. Combined with the experimental data, a theoretical model was established to evaluate and analyze the wellbore stability of Longmaxi formations shale under different working conditions of drilling, fracturing and completion. The results show that the shale of the Longmaxi Formation is a typical hard and brittle shale, the bedrock is dense, with high mechanical strength and weak hydration and expansion ability. The immersion effect of different working fluids has little influence on the expansion and mechanical properties of shale bedrock. However, the mechanical strength of shale with relatively developed bedding fractures is low, and the immersion effect of different drilling fluid further weakens the mechanical strength, resulting in obvious anisotropy of mechanical strength of underground rock. The coupling effect of seepage between wellbore and formation has obvious influence on the dynamic distribution of borehole pore pressure and wellbore stability under different working conditions. The effective fluid column pressure at the bottom of the hole is the highest during the fracturing process, which leads to the increase of pore pressure near the wellbore, and then to the increase of collapse pressure around the borehole wall. The equivalent density of collapse pressure rises to the maximum of 1.93 g/cm^3, and the wellbore stability is the worst in the fracturing process. The wellbore stability is secondary in the drilling process, and the wellbore stability is good when drilling along the direction of the maximum horizontal principal stress, and the equivalent density of collapse pressure is 1.69 g/cm^3. During the completion process, the formation fluid flows into the wellbore, the pore pressure in the borehole is relieved, and the equivalent density of the collapse pressure is reduced to approximately 1.35 g/cm^3, the wellbore stability is the best and open hole completion can be attempted in the horizontal well section. The results provide a certain theoretical reference for the selection of the drilling and completion schemes in shale formation.

1. Introduction

During the drilling process, the horizontal open hole section of the shale gas well is relatively long, and the seepage coupling effect between the wellbore rock and wellbore fluid and the change of effective stress field near the wellbore zone have a significant influence on the stability of the shale gas horizontal well (Liang et al., 2016; Zhao et al., 2016; Chen et al., 20181–3). In the process of fracturing, the shale gas

* Corresponding author. State Key Laboratory of Oil and Gas Reservoir Geology and Exploitation, Southwest Petroleum University, Southwest Petroleum University, Xindu Avenue 8#, Xindu District, Chengdu City, Sichuan, 610500, PR China.
** Corresponding author. State Key Laboratory of Oil and Gas Reservoir Geology and Exploitation, Southwest Petroleum University, Southwest Petroleum University, Xindu Avenue 8#, Xindu District, Chengdu City, Sichuan, 610500, PR China.
E-mail addresses: liuhoubin523@sina.com (H. Liu), cuishu8@sina.com, cuishu8@sina.com (S. Cui), mengyf523@sina.com, mengyf523@sina.com (Y. Meng), 522649874@qq.com (Z. Li), 1502263336@qq.com (X. Yu), 459260816@qq.com (H. Sun), 119059640@qq.com (Y. Zhou), 18602876494@163.com (Y. Luo).

https://doi.org/10.1016/j.petrol.2021.108882
Received 9 December 2020; Received in revised form 21 April 2021; Accepted 22 April 2021
Available online 26 April 2021

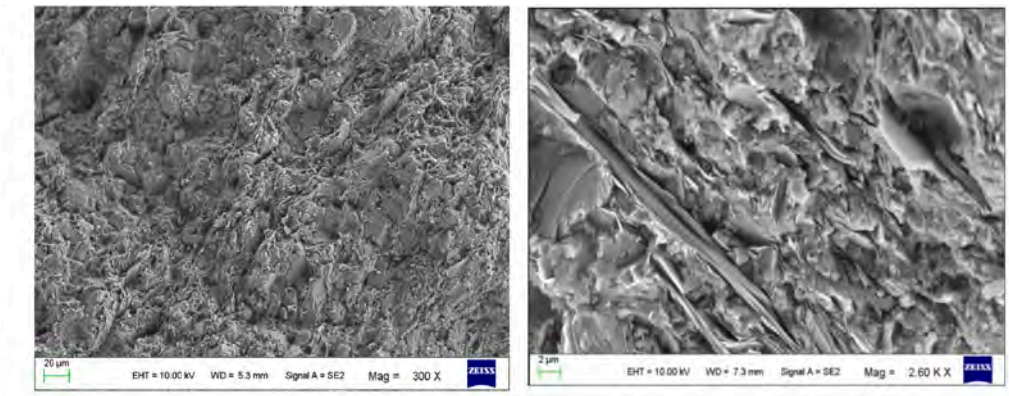

Fig. 1. Microstructure photo of the Longmaxi Formation shale.

reservoir is fractured on a large scale; the fracture interlaces and extends. The seepage effect of the fracture network near the well zone and the fluid–solid coupling effect with the rock mass influence the effective stress field around the shale gas reservoir and change the stability of the borehole wall (Ran et al., 2015).

Scholars worldwide have extensively investigated the borehole wall instability of drilling and completion in hard and brittle shale formations. Ma and Chen (2015) took the bedding and fracture weak plane as the research objects and integrated them with the mechanics-seepage coupling model by using weak bedding plane failure criterion to evaluate the failure mechanism of hard brittle shale formation. The damaged area around the horizontal well with different drilling times and different drilling directions were simulated and analyzed, and the critical equivalent mud density required to maintain the wellbore stability in different periods was calculated. Shale exhibits a high degree of elastic anisotropy because of its bedding characteristics and often reacts chemically to the drilling fluid. Kanfar et al. (2017) established a force–chemical–seepage coupling borehole wall stability analysis model for the reduction of mechanical strength and additional hydration stress after the mud shale was soaked by the drilling fluid. This model could be used to evaluate the borehole wall stability that varied with time during and after drilling. Chen et al. (2019) regarded the micro-cracks as the damage of the hard and brittle shale from the perspective of the micro-cracks of the hard and brittle shale. The distribution of the micro-cracks was determined by a random function, and the damage mechanics and fracture mechanics were combined to establish the damage constitutive model of the hard and brittle shale. The FLAC3D software was used to simulate and analyze the wellbore stability, and the results showed the sensitivity of hard brittle shale to drilling fluid; the development degree of micro-fractures had the greatest influence on the wellbore stability. The plugging property and density of drilling fluids are important means of ensuring the stability of hard brittle shale. Ding et al. (2018) established a new model for shale formations with a relatively developed weak plane to study the influence of multiple groups of weak planes on the wellbore stability in shale formations. This model was used to analyze the influence of the weak plane on the stress distribution and shale strength. The results proved that the existence of the weak plane reduces the strength of the shale, and the collapse pressure increases with the increase of anisotropy of shale formation. For horizontal wells, choosing a suitable drilling azimuth can reduce the impact of the weak plane on the wellbore stability. Fan et al. (2013) established a model for analyzing the strength of the metamorphic rock formation with well logging data based on the results of the core mechanics experiments in metamorphic formations. The minimum bottomhole flow pressure needed to stabilize the borehole was calculated by using the borehole completion stability analysis method, and the maximum allowable production pressure difference was obtained to judge the feasibility of the open-hole completion method. Wen et al. (2014) established a coupling model of the borehole wall stability in an inclined section of the hard and brittle shale by considering the structural characteristics and weak surface hydration; they used the model to analyze the influencing factors of the collapse pressure distribution. The established coupling model can predict the collapse pressure more accurately.

In the above studies, researchers had not formed a complete set of evaluation methods for wellbore stability during the drilling, fracturing, and completion processes. Therefore, we conducted systematic laboratory tests on Longmaxi shale in a block in China and incorporated these results into an established theoretical model to evaluate the dynamic changes of the wellbore-stratum seepage field, effective stress field, and wellbore stability during the drilling, fracturing, and completion processes. It can provide theoretical support for the formulation of the shale gas well development plan, optimize engineering design, and provide efficient on-site construction in this area.

2. Materials

The research object of this paper is the Longmaxi Formation shale in a certain block in China, and the average depth of the underground core was more than 3500 m. We used x-ray diffraction (XRD) equipment to measure the mineral composition and content distribution of the downhole cores, which was mainly composed of brittle minerals, such as calcite and quartz, with a quartz content of approximately 46% and a small amount of feldspar (An et al., 2020). The clay mineral content was approximately 34% and was mainly composed of illite, chlorite, and other clay minerals with weak expansion ability; the shale contained a small amount of imonite mixed layer; however, the mixed layer ratio was very low. This implies that the Longmaxi Formation shale was hard and brittle shale with weak hydration and expansion capacity (Rick et al., 2008). In general, this type of shale has high hardness, strong brittleness, and weak hydration expansion ability. The shale microstructure characteristics of Longmaxi Formation are shown in Fig. 1.

Fig. 1 shows that the Longmaxi Formation shale is dense; however, it is hard and brittle in nature with relatively developed bedding cracks and relatively uniform trends of micro-fractures.

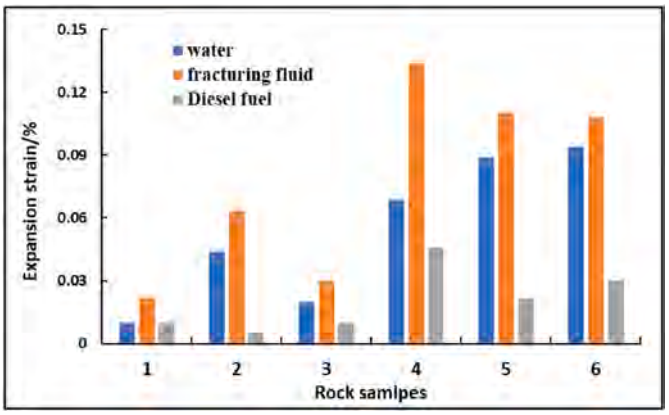

Fig. 2. Shale expansion performance test results of Longmaxi Formation.

Table 1
Testing results of porosity and permeability parameters in the Longmaxi Formation.

Core number	Length [cm	Diameter [cm]	Porosity [%]	permeability [mD]
8-18-69-1	4.4080	2.5120	0.56	0.0000490
8-18-69-2	4.2920	2.5420	0.46	0.0001024
8-18-69-3	4.2800	2.5410	0.64	0.0001147
7-95-117-1	4.4160	2.5340	0.55	0.0011540

3. Experimental methods and results

3.1. Physical and chemical performance parameters test of shale

Hydration expansion performance test can be used to evaluate the expansion performance of downhole rock samples under different immersion systems. This test can be used to evaluate the inhibition ability of the rock mass expansion by using different drilling fluid systems and is a way of optimizing the drilling fluid system (Barati et al., 2016). This test can also evaluate the expansive property of the rock and analyze the hydration expansive ability of the rock on the borehole wall; the mechanism of the borehole wall collapse and instability can also be measured. The downhole cores with similar homogeneity after screening were respectively put into the hydration expansion tester equipped with different working fluids, and the hydration and expansion performance of downhole shale under the environment of on-site working fluid immersion was evaluated and analyzed after the same immersion time. The test results are shown in Fig. 2.

Fig. 2 shows that the shale expansion of the Longmaxi Formation is very small under different drilling fluid environments, and the expansion strain is generally less than 0.1%. The expansion strains of the different drilling fluids are as follows:

(i) The expansion strain of the fracturing fluid is greater than that of the aqueous solution;
(ii) The expansion strain of the aqueous solution is greater than that of the diesel oil; and
(iii) The hydration expansion capacity of shale in the Longmaxi Formation is weak.

When combined with the X-ray powder diffraction test results, this type of shale usually has high hardness, strong brittleness, and weak hydration expansion capacity, and it is prone to produce micro-cracks under high stress and external forces.

The test of porosity and permeability performance parameters of rock can be used to evaluate the permeability capacity of borehole rock and to provide the basic parameters for the dynamic change law of the permeability field and stress field between the wellbore and stratum in later stages. The porosity and permeability of shale in Longmaxi Formation were measured by the tight rock gas permeability tester in the laboratory. The test results are shown in Table 1 and Table 2.

Tables 1 and 2 show that the porosity and permeability of shale in the Longmaxi Formation are relatively low, and the permeability is generally 10^{-4}–10^{-2} mD. The permeability in the direction of the parallel bedding is higher than that in the direction perpendicular to the bedding, which proves that the conductivity of the bedding cracks was higher than that of the shale bedrock.

3.2. Testing and analysis of shale mechanical properties

The systematic triaxial mechanics test accurately obtains the mechanical parameters of rocks under the downhole pressure environment; this information can be used to evaluate the influences of different drilling fluid systems, fracture developments, fracture strikes, and other factors on the mechanical properties of borehole rocks (Wang et al., 2018). The shale of the Longmaxi Formation was developed with bedding fractures. Based on this information, the shale of Longmaxi Formation was used with different bedding trends to conduct triaxial experiments under different confining pressures. The experimental results are shown in Fig. 3.

Fig. 3 shows that the anisotropic characteristics of elastic parameters and the mechanical strength of the bedding shale are obvious. Due to the existence of bedding cracks, the elastic modulus of the rock samples perpendicular to the direction of bedding cracks is small, and the compressive strength of the rock samples parallel to the direction of bedding is low. In addition, the rock samples parallel to the direction of the bedding are prone to fracture failure along the bedding cracks.

At the same time, the triaxial mechanical testing machine was used to test the mechanical parameters of the shale after soaking in different working fluids under the confining pressure of 45 MPa. The main components of the fracturing fluid used in the field are glue, friction reducer water and activated water, and the main completion fluid used is the water-based completion fluid. The experimental results are shown in Fig. 4.

Fig. 4 shows that, on the whole, the field oil-base drilling fluid, fracturing fluid, and completion fluid have no obvious influence on the mechanical properties of the shale in the Longmaxi Formation. The elastic modulus and compressive strength of some rock samples decreased slightly after immersion in the completion fluid and fracturing fluid, but the decrease was small. The variation in the shale mechanical properties under oil-based drilling fluid was not obvious, which implies that the immersion effect of different working fluids has little influence on the shale's mechanical properties. However, for the rock samples of

Table 2
Testing results of porosity and permeability parameters of Well 1 in the Longmaxi Formation.

Formation		Horizontal permeability [mD]			Vertical permeability [mD]		
		Range	Average value	Amount	Range	Average value	Amount
Longyi section	④	0.0012–0.0038	0.0025	2	0.000129–0.000054	0.000091	2
	③	0.0144–0.0144	0.0144	1	0.000013–0.000171	0.000092	2
	②	0.0178–0.0178	0.0178	1	0.000937–0.000937	0.000937	1
Wufeng formation	①	0.0025–0.0093	0.0052	3	0.000081–0.004014	0.001451	3

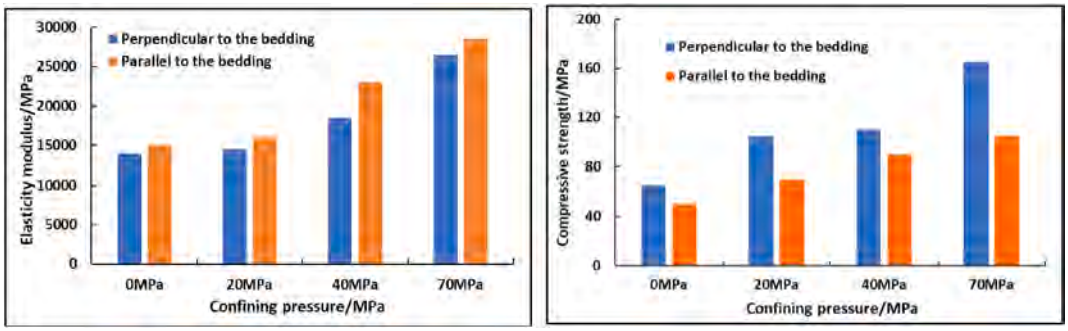

Fig. 3. Triaxial experimental results of shale with different bedding trends in Longmaxi Formation.

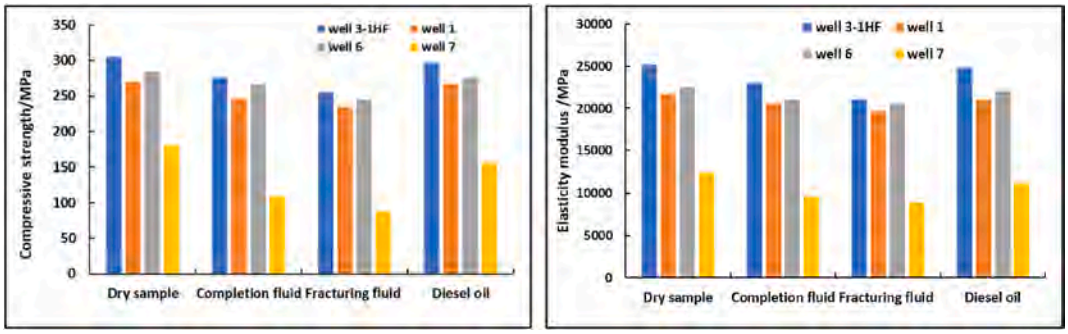

Fig. 4. Triaxial test results of Longmaxi shale after soaking in drilling fluid.

Well 7 that developed bedding cracks, the effect of working fluid immersion had a significant effect on the mechanical strength of the rock. When the working fluid penetrates along the fractures under the downhole pressure, the induced splitting effect makes it likely for the rock samples to be destroyed along the bedding fractures.

4. Theory and calculation

4.1. Dynamic distribution law of wellbores: Formation seepage field and pore pressure during drilling and completion

In this paper, we established a theoretical model of the dynamic change rules of the wellbore formation's seepage field, effective stress field, and wellbore stability in the horizontal section of the Longmaxi Formation shale during the drilling, fracturing, and completion processes by considering the wellbore trajectory, bedding fracture direction, pressure penetration, hydration effect, mechanical strength loss under anisotropy of mechanical properties, and so on. Firstly, the quantitative model of borehole porosity and permeability in horizontal shale wells was established.

(1) The mathematical model of wellbore pore pressure transfer is shown as follows (Ma et al., 2016):

$$\frac{\partial P}{\partial t} = k^* \nabla^2 P + \sum_{i=1}^{N} \nabla\left(D_i^* \nabla c_{c_i}^*\right) \tag{1}$$

$$\frac{\partial c_i}{\partial t} = \frac{k}{\mu \varphi_0}\left[\nabla(\lambda_i c_i)\cdot\nabla P + \lambda_i c_i \nabla^2 P\right] + \frac{1}{\varphi_0}\nabla(D_i \nabla c_i) \tag{2}$$

where P is the formation pore pressure in MPa; K^* is an effective (dimensionless) permeation coefficient; K is the formation permeability in mD; D_i^* is the multicomponent mineral effective diffusion coefficient in cm^2/s; D_i is the effective diffusion coefficient of one component mineral in cm^2/s; c_i is the molality concentration of one component mineral in mol/L; C_i^* is the molality concentration of multicomponent minerals in mol/L; μ is the viscosity in Pa·s; φ_0 is the porosity in %; and λ_i is the (dimensionless) coupling coefficient.

(2) The mathematical model of the radial flow capacity of a borehole wall is as follows (Ma et al., 2016):

$$k_R = k_{11} sin^2\theta_1 + k_{33} cos^2\theta_1 = \frac{k_{11}+k_{33}}{2} - \frac{k_{11}-k_{33}}{2} cos2\theta_1 \tag{3}$$

where K_R is the radial flow capacity of the borehole wall in D; K_{11} and K_{33} are the permeability components in three-dimensional space in D; θ_1 is the angle between the bedding plane and the X-axis in degrees.

(3) The accurate evaluation of the angle relationship between the main stress field of the wellbore and the normal direction of the bedding surface is key to evaluating the wellbore stability of drilling horizontal wells in bedding shale reservoirs (Jin and Chen, 2012). The relationship between the radial direction of the borehole wall and the normal angle of the bedding plane is as follows:

$$\xi = \arccos\left(\frac{a_1\cdot b_1 + a_2\cdot b_2 + a_3\cdot b_3}{\sqrt{a_1{}^2 + a_2{}^2 + a_3{}^2}\cdot\sqrt{b_1{}^2 + b_2{}^2 + b_3{}^2}}\right)\cdot\frac{180}{\pi} \tag{4}$$

Here,

$$a_1 = \sin\alpha_s \cos\beta_s$$
$$a_2 = \sin\alpha_s \sin\beta_s$$
$$a_3 = \cos\alpha_s$$
$$b_1 = \cos\beta\cos\alpha\cos\theta - \sin\beta\sin\theta$$
$$b_2 = \sin\beta\cos\alpha\cos\theta + \cos\beta\sin\theta$$
$$b_3 = -\sin\alpha\cos\theta$$

where ξ is the included angle between radial flow direction and fracture plane of borehole wall in degrees; α_s is fracture dip angle in degrees; β_s is fracture tendency in degrees; $\alpha$is the inclination angle of the well trajectory in degrees; β is the azimuth angle of the wellbore trajectory in degrees; and θ is the well circumference angle in degrees.

Based on the included angle relationship between the main stress field of the borehole wall and the normal direction of the bedding surface established above, the influence of the bedding strike, dip angle, and wellbore trajectory on the included angle relationship between the

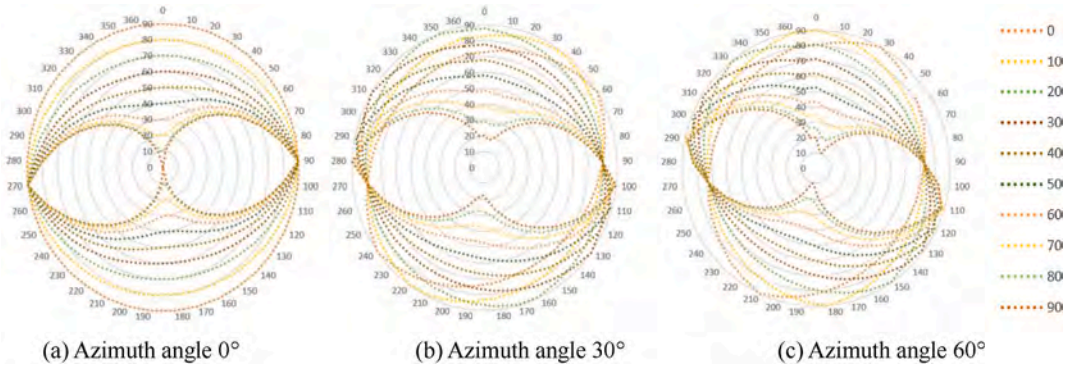

Fig. 5. Variation law of the angle between the radial seepage direction of the wellbore and bedding plane.

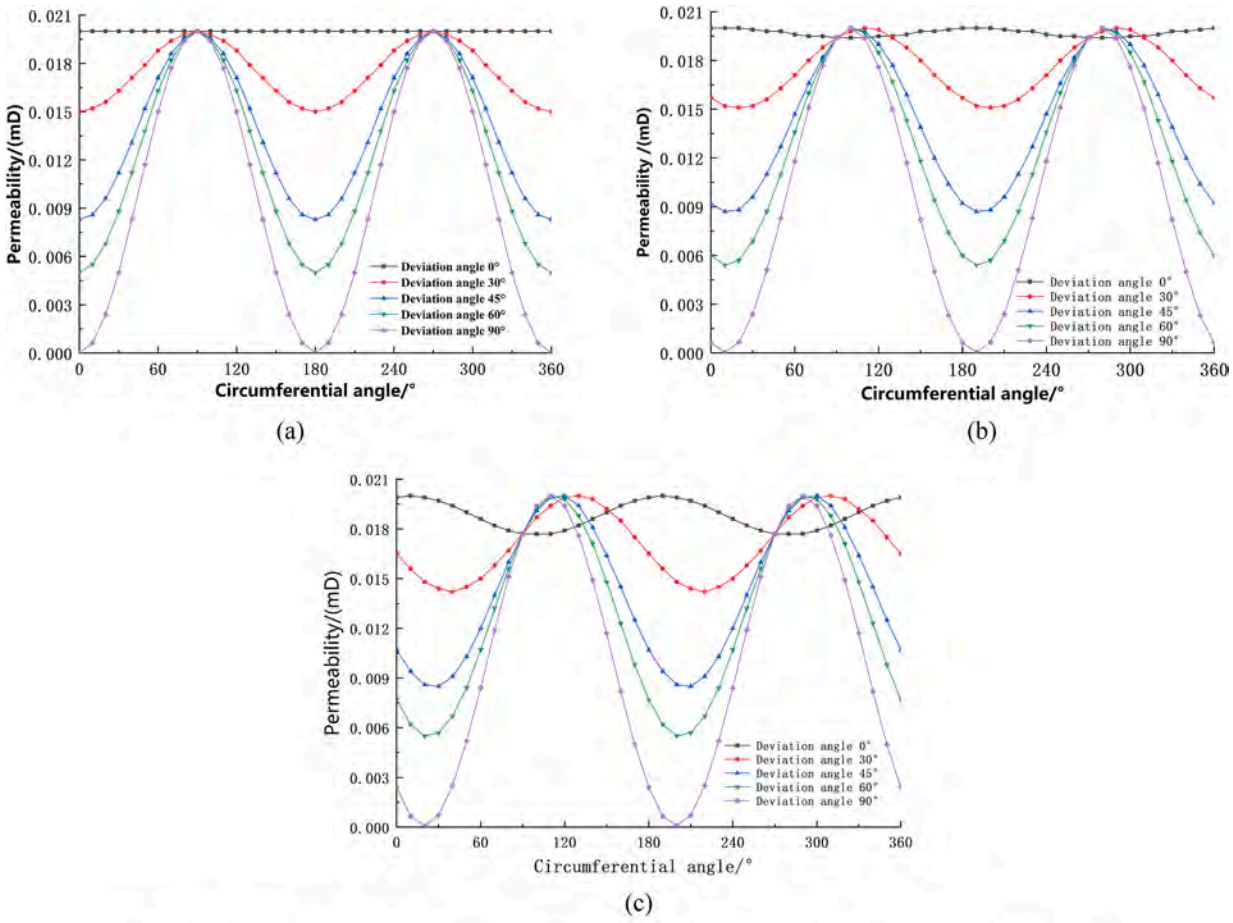

(a) The borehole trajectory azimuth angle is 90°, and the crack inclination is 0°; (b) The borehole trajectory azimuth angle is 90°, and the crack inclination is 10°; (c) The borehole trajectory azimuth angle is 90°, and the crack inclination is 20°

Fig. 6. Variation law of seepage around a well at different fracture inclinations.

main stress field of the borehole wall and the normal direction of bedding were evaluated (see Fig. 5)

Fig. 5 shows that the well inclination angle and azimuth angle have obvious effects on the permeability near the borehole wall of the stratigraphic shale reservoir. Under the same azimuth angle and inclination angle, the borehole wall permeability changes significantly with changes in the well circumference angle. This shows that when the bedding strike and inclination angle are constant, the azimuth angle, inclination angle, and circumferential angle affect the included angle relationship between the wellbore seepage direction and the bedding surface.

Similarly, for the test results of the porosity and permeability parameters of the Longmaxi Formation Well 1, we consider the angle relationship between the radial seepage direction and the bedding surface of the borehole wall of the bedding shale reservoir. During the drilling process, the permeability mathematical description method of

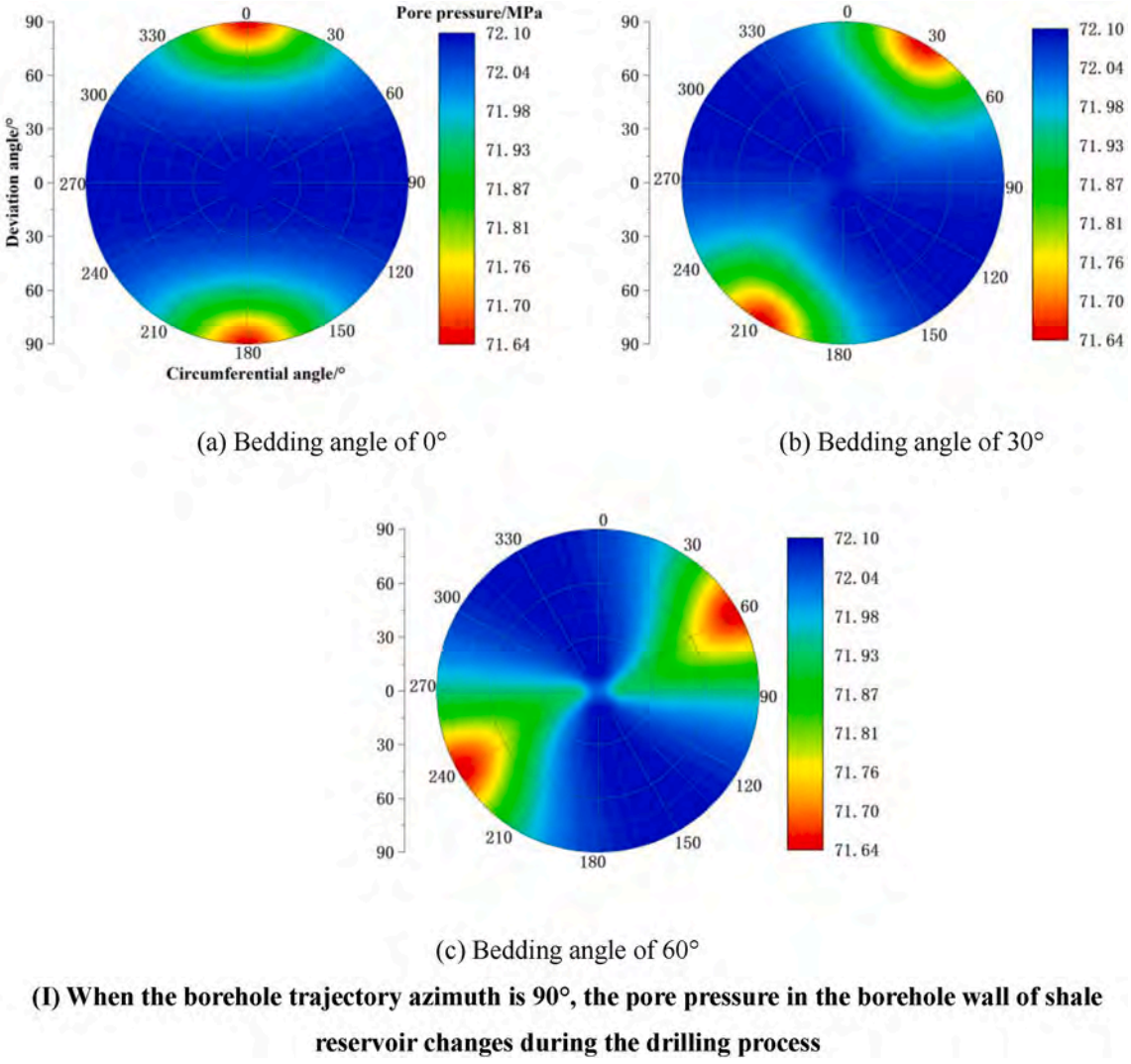

Fig. 7. Variation law of borehole pore pressure in shale reservoir during drilling and completion of Well 1.

the anisotropic formation established above was used to evaluate the permeability change rules of the borehole wall under different azimuth angles, inclination angles, and well circumference angles (see Fig. 6).

Fig. 6 shows that there are differences in the seepage capacity of the shale reservoir during drilling. When the bedding is horizontal, and the borehole trajectory azimuth is 90°, the inclination angle is 0°, that is, when drilling in a straight section, each point around the well is radially parallel to the bedding fracture, and the permeability is 0.02 mD. With the increase in the inclination angle, the angle between the radial direction and the strike of the bedding fracture surface changes at each location point around the well. When the inclination angle is 90° (i.e., in the horizontal well section) and the circumferential angle is 90° (or 270°), the radial seepage capacity of the borehole wall is the maximum; when the circumferential angle is 0° (or 180°), the radial seepage capacity of the borehole wall is the least. The seepage capacity of the borehole wall in the shale formations is related to the angle between the bedding fracture surface and the borehole axis. The seepage capacity parallel to the bedding surface is high, and the seepage capacity perpendicular to the bedding surface is the least.

Similarly, the pressure in the radial seepage capacity of the borehole rock will inevitably lead to differences in the seepage capacity between the wellbore and formation under the bottom hole pressure environment and between the pore pressure distribution and effective stress field near the borehole wall. Taking the Longmaxi Formation Well 1 as an example, the pore pressure distribution of the borehole wall during the drilling process and the completion and production processes were evaluated and analyzed. The pore pressure gradient of Well 1 in the Longmaxi Formation was 59.6 MPa; the bottom hole liquid column pressure during the drilling process was 63.4 MPa, and the bottom hole flowing pressure of the test production was 39.22 MPa. The evaluation results are shown in Fig. 7.

Fig. 7 shows that fluid migration between the wellbore and the formation has a significant effect on the pore pressure in the formation around the well during the drilling and completion processes. In the process of drilling, the wellbore pressure is higher than the formation pore pressure, and the drilling fluid migrates to the formation, which increases the borehole pressure in the borehole wall. However, the increase in amplitude is different at different positions around the well and depends on the angle relationship between the radial direction of each point and the bedding surface. In the process of completion, the wellbore pressure is lower than the formation pore pressure; the formation fluid flows into the wellbore, and the pore pressure in the wellbore decreases. The variation amplitude of the pore pressure in the wellbore depends on the radial seepage capacity of the rock in the wellbore.

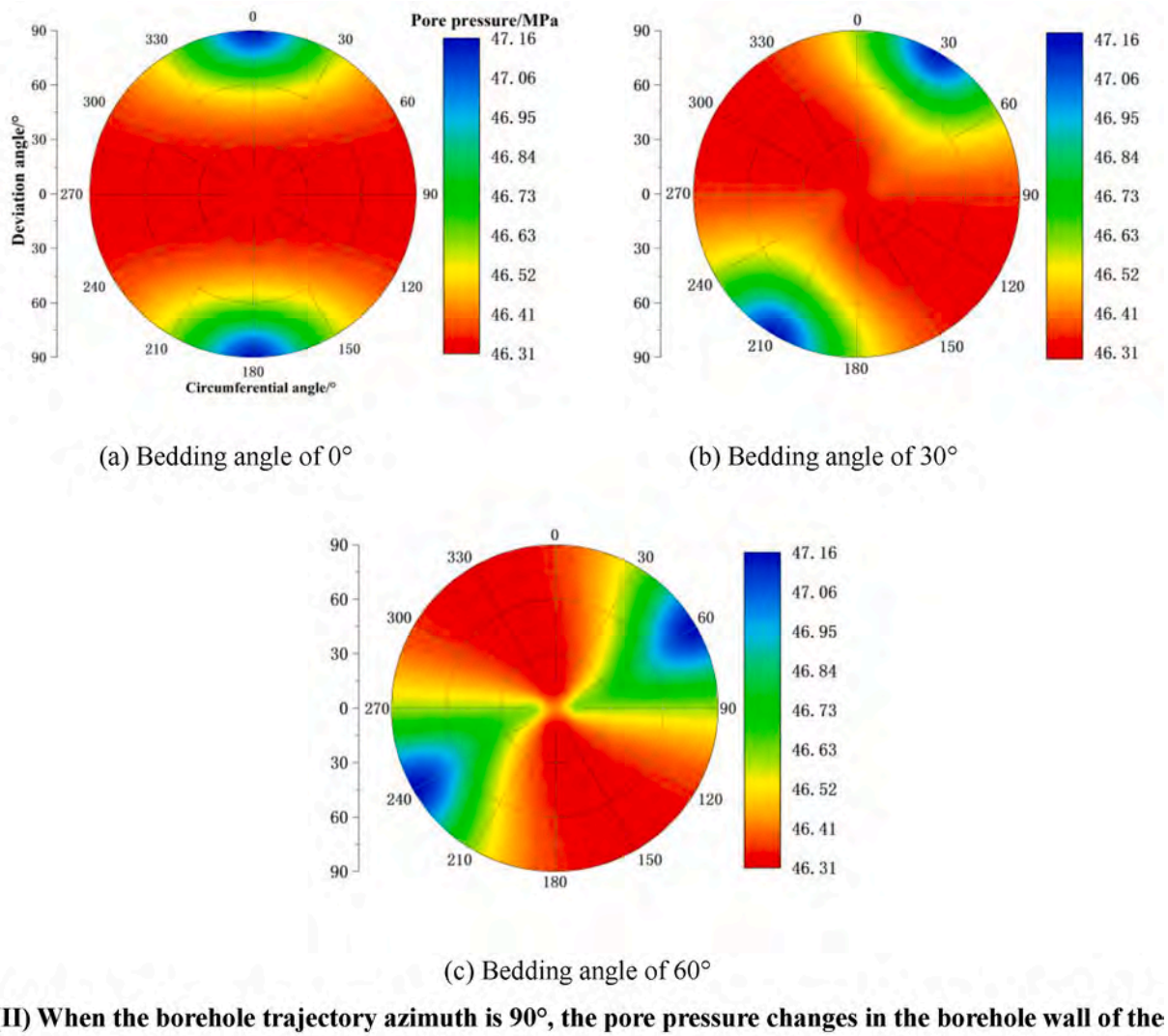

(a) Bedding angle of 0°

(b) Bedding angle of 30°

(c) Bedding angle of 60°

(II) When the borehole trajectory azimuth is 90°, the pore pressure changes in the borehole wall of the shale reservoir during completion production

Fig. 7. (*continued*).

4.2. Dynamic distribution law of seepage field and pore pressure in the fracturing area

The permeability of the shale reservoir is low. To increase the reservoir permeability, complex networks of artificial fractures often need to be created by fracturing stimulations. After the formation of artificial fractures, the natural fractures and the connections between them and the wellbore will be communicated, which leads to liquid phase intrusions into the deep reservoir along the artificial fractures (Wu et al., 2012). The seepage model of the shale reservoir during fracturing is established by the motion equation, state equation, and continuity equation. To obtain the basic equations of liquid seepage for the shale formation matrix and the fracture system, we considered the interfacial flow between the matrix and the fracture and substituted the equation of motion and the equation of state into the equation of continuity.

The matrix and liquid phase equation is as follows:

$$\rho_w \frac{k_m}{\mu_w}\nabla^2 p_m = -\frac{\partial(\varphi_m \rho_w)}{\partial t} + \frac{\alpha_1 k_{nf}}{\mu_w}(p_{nf} - p_m)\rho_w + \frac{\alpha_3 k_{hf}}{\mu}(p_{hf} - p_m)\rho_w + \frac{k_m}{\mu_w r}(p_{well} - p_m)\rho_w \quad (5)$$

The natural fracture equation is as follows:

$$\rho_w \frac{k_{nf}}{\mu_w}\nabla^2 p_{nf} = -\frac{\partial(\varphi_{nf} \rho_w)}{\partial t} + \frac{\alpha_2 k_{hf}}{\mu_w}(p_{hf} - p_{nf})\rho_w - \frac{\alpha_1 k_{nf}}{\mu_w}(p_{nf} - p_m)\rho_w + \frac{k_{nf}}{\mu_w r}(p_{well} - p_{nf})\rho_w \quad (6)$$

The artificial fracture equation is as follows:

$$\rho_w \frac{k_{hf}}{\mu_w}\nabla^2 p_{hf} = -\frac{\partial(\varphi_{hf} \rho_w)}{\partial t} - \frac{\alpha_2 k_{hf}}{\mu_w}(p_{hf} - p_{nf})\rho_w - \frac{\alpha_3 k_{hf}}{\mu_w}(p_{hf} - p_m)\rho_w + \frac{k_{hf}}{\mu_w r}(p_{well} - p_{hf}) \quad (7)$$

The first term on the right of the equation represents the change rate of the volume of the rock skeleton caused by the change of the seepage pressure. The second item represents the interflow term between the substrate and the fracture system. The third term represents the seepage flow from the wellbore to the matrix.

The initial conditions and boundary conditions of the seepage equation are as follows:

$$\begin{cases} p_m(r,0) = p_{hf}(r,0) = p_{nf}(r,0) = p_0 \\ p_m(+\infty,t) = p_{hf}(+\infty,t) = p_{nf}(+\infty,t) = p_0 \\ p_m(r_w,t) = p_{hf}(r_w,t) = p_{nf}(r_w,t) = p_{well} \end{cases} \quad (8)$$

Fig. 8. COMSO geometric model after fracturing to form artificial fractures.

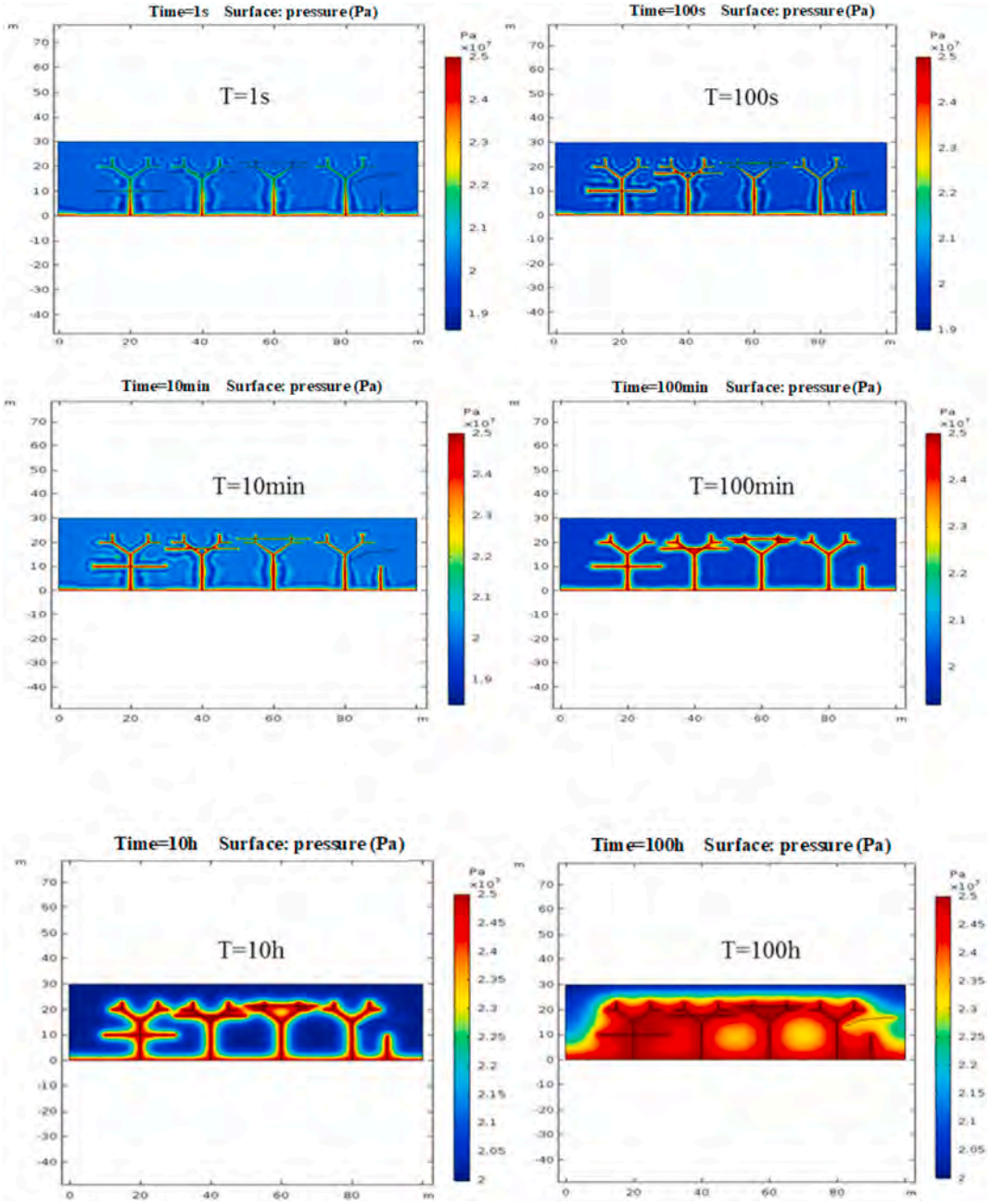

Fig. 9. Pressure contour plots of the matrix and fracture system at different times.

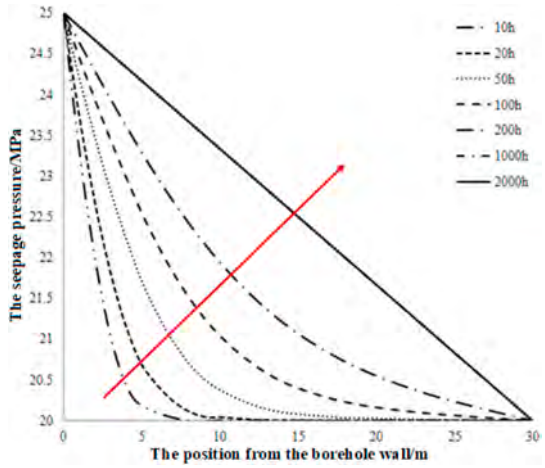

Fig. 10. Evolution of matrix seepage pressure after artificial fracture formation.

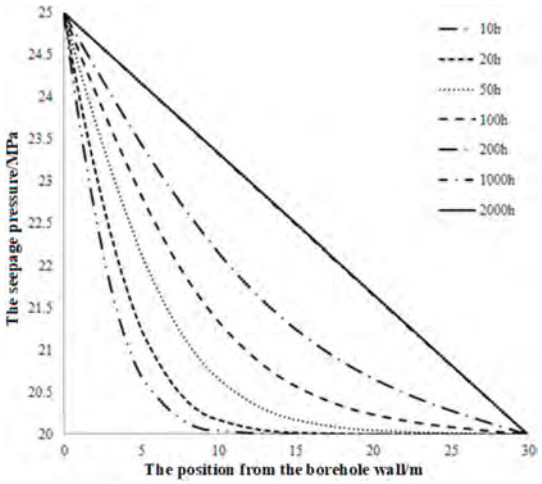

Fig. 11. Evolution process of the seepage pressure in the natural fractures after the formation of artificial fractures.

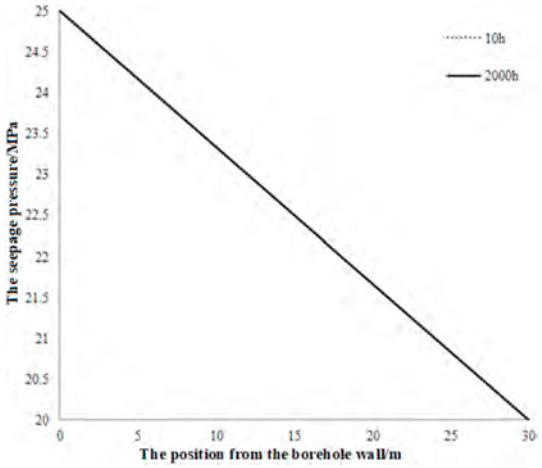

Fig. 12. Seepage pressure evolution process of artificial fractures.

where ρ_w is the density of the drilling fluid in g/cm^3; k_m is the equivalent permeability of the shale matrix in um^2; μ_w is the viscosity of the water phase in Pa·s; P_m is the internal pressure of the matrix in MPa; φ_m is the porosity of the shale matrix in %; k_{nf} is the equivalent permeability of natural fractures in um^2; P_{nf} is the internal pressure of natural fractures in MPa; k_{hf} is the absolute permeability of the artificial fractures in um^2; P_{hf} is the liquid column pressure of the artificial fractures in MPa; p_{well} is the static water column pressure in MPa; φ_{nf} is the porosity of natural fractures in %; α_1 is the flow factor from natural fractures to the matrix; α_2 is the flow factor from the artificial fractures to natural fractures; α_3 is the channeling flow factor from artificial fractures to the matrix; r is the seepage distance, where it can also represent the distance from the wellbore to the seepage node in m; r_w is the borehole radius in m; φ_{hf} is the porosity of the artificial fracture in %; and P_0 is the initial pressure of the formation in MPa.

According to the physical model of the artificial fracture, after the completion process was invaded by the fracturing fluid, the geometric model was established in COMSOL (see Fig. 8). Fig. 8 established a shale matrix with a width of 100 m and a length of 30 m. To simulate the wellbore, the pressure at the bottom of the model was set to be constant at *Pw*. The pressure at the top of the model was constant at P_0 to simulate the infinity of the formation. Four artificial fractures were set in the matrix; the artificial fractures developed branch fractures, and three of them were penetrated by natural fractures. There were two other natural fractures that did not meet the artificial fractures, but one of them was connected to the wellbore.

The seepage control equation after the formation of fracturing cracks consists of basic equations and their initial and boundary conditions. Fig. 9 shows the pressure cloud map of the matrix and fracture system simulated and analyzed at different times.

From Fig. 9, it can be seen that the permeability of the artificial fracture is much higher than the permeabilities of the matrix and natural fractures; therefore, the liquid phase penetrates rapidly along the artificial fracture in the initial stage of the liquid phase invasion. After reaching the boundary of the artificial fracture, the liquid phase begins to invade along the natural fracture. At the same time, the liquid phase flows slowly to the matrix around the artificial fracture. During this period, the liquid phase invades the matrix under the pressure difference between the wellbore liquid column pressure and formation pore pressure. However, because of its low permeability and the influence of the dominant role of fractures on seepage, the liquid inflow rate in the matrix is slow. After the liquid phase continues to invade along the natural fracture for a period, the pore pressure in the natural fracture gradually increases, and under the pressure difference, the liquid phase flows from the natural fracture to the matrix. As the liquid content of the matrix increases, the pore pressure of the matrix also increases. When the pressure between the matrix and the fracture system tends to be stable, the pressure front will advance smoothly along the depth of the formation. It can also be observed from the pressure cloud map that the two natural fractures that do not intersect with the artificial fractures show different pressure evolution processes; the pressure evolution speed of the natural fractures that are connected with the wellbore is weaker than that of the artificial fractures at the moment of fluid intake. However, due to the differential pressure drive between the wellbore and the formation, the liquid phase will quickly invade the natural fractures. However, a natural fracture that is not connected with the artificial fracture or the wellbore shows poor communication with the fluid and slow evolution of the seepage pressure velocity. This is clear from the fact that the natural fracture that is not connected with artificial fracture or the wellbore in the production process does not contribute much to productivity improvement.

The seepage pressure evolution process of the matrix is calculated as shown in Fig. 10.

The seepage pressure evolution process of natural fractures is shown in Fig. 11.

The seepage pressure evolution process of artificial fractures is shown in Fig. 12.

The evolution process of the matrix seepage pressure caused by the liquid phase intrusion in the drilling process is slower than the evolution process of the natural fracture seepage pressure after the formation of

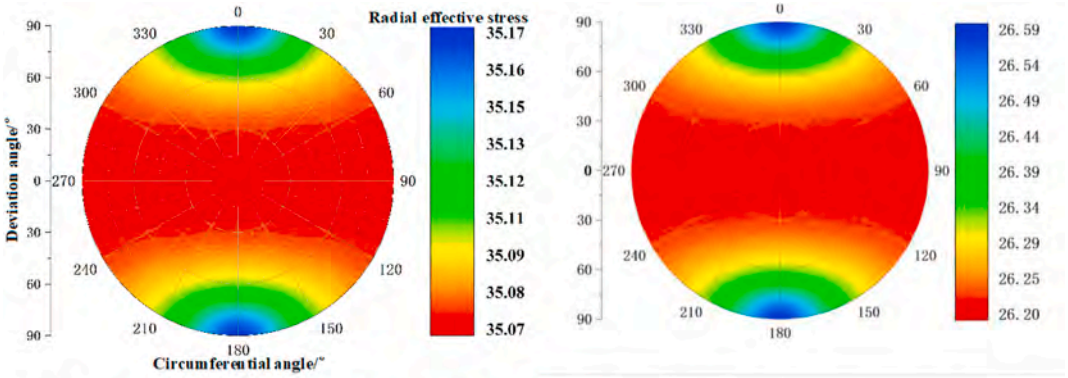

(a) Radial effective stress distribution during drilling process (b) Radial effective stress distribution during fracturing process

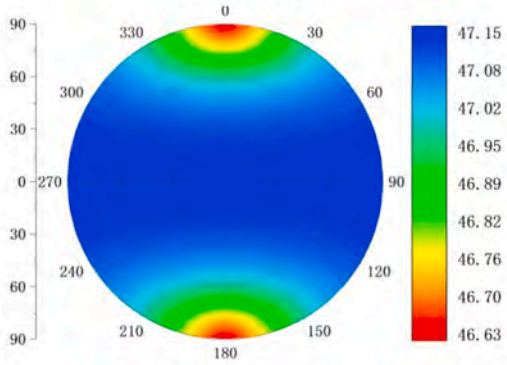

(c) Radial effective stress distribution during the completion production process

Fig. 13. Distribution of effective radial stress field on borehole wall of shale reservoir in Longmaxi Formation.

the artificial fracture. The evolution trend of the seepage pressure with the radial distance at 10 h is close to coincidence with that at 2000 h. This is due to the high permeability of the artificial fractures, which enable the liquid phase to enter the shale formation and permeate quickly. The front edge of the liquid phase breaks through to the intersection of the artificial fractures and natural fractures in a short time. At this point, the liquid phase enters the natural fracture. The starting pressure gradient of the liquid phase at this moment is less than that required by the liquid phase to enter the natural fracture during the drilling process. Therefore, the liquid phase enters the natural fracture from the artificial fracture faster than it enters the natural fracture from the wellbore and matrix during the drilling process.

4.3. Dynamic change rules of effective stress field and wellbore stability during the drilling, fracturing, and completion

For directional wells or horizontal wells, it is necessary to consider the influence of factors such as the wellbore trajectory (inclination angle and azimuth angle) and radial seepage of the borehole rock. Combining the well trajectory inclination angle α, azimuth angle β, and the in-situ stress field (σ_H, σ_h. σ_v) in the rectangular coordinate system, the cartesian coordinate transformation can be used to obtain the stress field (σ_x, σ_y, σ_z, τ_{xy}, τ_{xz}, τ_{yz}) of the borehole axis in the rectangular coordinate system for any azimuth and inclination. The transformation relationship can be expressed as follows (Chen, 2008):

$$\begin{aligned}
\sigma_x &= \cos^2\alpha\left(\sigma_H\cos^2\beta+\sigma_h\sin^2\beta\right)+\sigma_V\sin^2\beta\\
\sigma_y &= \sigma_H\sin^2\beta+\sigma_h\cos^2\beta\\
\sigma_z &= \sin^2\alpha\left(\sigma_H\cos^2\beta+\sigma_h\sin^2\beta\right)+\sigma_V\cos^2\alpha\\
\tau_{xy} &= \cos\alpha\sin\beta\cos\beta(\sigma_h-\sigma_H)\\
\tau_{xz} &= \cos\alpha\sin\alpha\left(\sigma_H\cos^2\beta+\sigma_h\sin^2\beta-\sigma_V\right)\\
\tau_{yz} &= \sin\alpha\cos\beta\sin\beta(\sigma_h-\sigma_H)
\end{aligned} \tag{9}$$

Under the cylindrical coordinate system, the effective stress field on the sidewall surface of any inclined well ($r = r_w$) can be expressed as follows:

$$\begin{aligned}
\sigma_r &= p_w - ap(r,t)\\
\sigma_\theta &= \left(\sigma_x+\sigma_y\right)-p_w-\left(\sigma_x-\sigma_y\right)\cos 2\theta-4\times\tau_{xy}\times\sin 2\theta-ap(r,t)\\
\sigma_{zz} &= \sigma_z-\mu\left[2\left(\sigma_x-\sigma_y\right)\cos 2\theta+4\tau_{xy}\sin 2\theta\right]-ap(r,t)\\
\tau_{\theta z} &= 2\left(-\tau_{xz}\sin\theta+\tau_{yz}\cos\theta\right)\\
\tau_{r\theta} &= \tau_{rz}=0
\end{aligned} \tag{10}$$

where σ_H is the horizontal maximum principal stress in MPa; σ_h is the minimum horizontal principal stress in MPa; σ_V is the vertical principal stress in MPa; σ_x, σ_y, σ_z, τ_{xy}, τ_{xz}, τ_{yz} are the components of the ground stress in MPa; and σ_r, σ_θ, σ_{zz}, $\tau_{\theta z}$, $\tau_{r\theta}$ are the stress components in cylindrical coordinates (MPa). P_w is the liquid column pressure in MPa; α is the borehole trajectory inclination angle in degrees; β is the borehole trajectory azimuth angle in degrees; θ is the well circumference angle in degrees; μ is the dimensionless Poisson's ratio; a is the dimensionless effective stress coefficient; and p(*r,t*) is the formation static pore pressure at the time *t* when the distance from the borehole wall is *r* measured in MPa.

For formations with beddings and fractures, the mechanical weak surface criterion can be used to evaluate and analyze the influence of the weak surface on the stability of the borehole wall. In this paper, the Jaeger model was used to characterize the impact of the weakness of the rock mechanics on the rock mass mechanical properties (Jaeger and Cook, 1979). This model describes the shear failure conditions of a rock mass with one or a group of parallel weak planes; therefore, it is usually referred to as a single group of the weak plane strength theoretical model. In this model, the failure criterion of the weak plane is as follows (Chen, 2008):

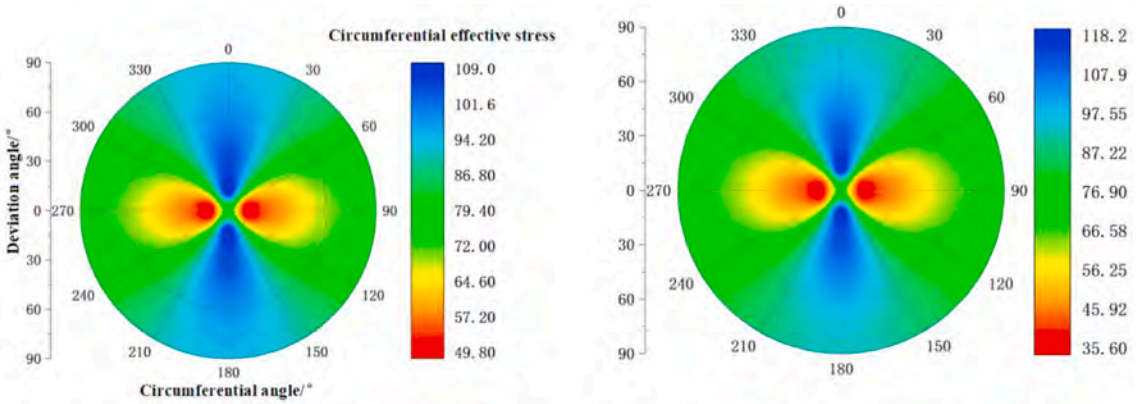

(a) Circumferential effective stress distribution during drilling process (b) Circumferential effective stress distribution during the fracturing process

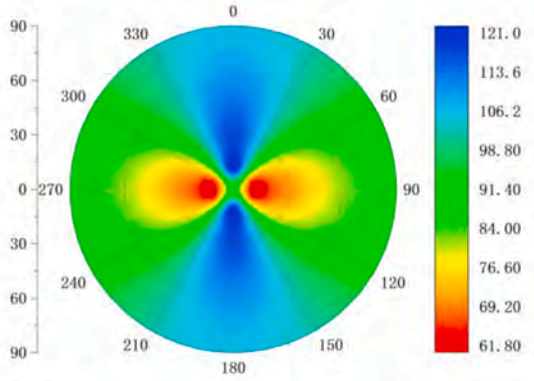

(c) Circumferential effective stress distribution during the completion production process

Fig. 14. Distribution of effective circumferential stress field on borehole wall of shale reservoir in Longmaxi Formation.

$$\sigma_1 = \sigma_3 + \frac{2(C_w + \sigma_3 \tan\phi_w)}{(1 - \tan\phi_w \cot\beta_0)\sin 2\beta_0} \quad (\beta_1 \le \beta_0 \le \beta_2) \tag{11}$$

Here,

$$\begin{cases} \beta_1 = \dfrac{\phi_w}{2} + \dfrac{1}{2}\arcsin\left[\dfrac{(\sigma_1 + \sigma_3 + 2C_w \cot\phi_w)\sin\phi_w}{\sigma_1 - \sigma_3}\right] \\ \beta_2 = \dfrac{\pi}{2} + \dfrac{\phi_w}{2} - \dfrac{1}{2}\arcsin\left[\dfrac{(\sigma_1 + \sigma_3 + 2C_w \cot\phi_w)\sin\phi_w}{\sigma_1 - \sigma_3}\right] \end{cases} \tag{12}$$

If the above conditions are not met, the rock mass failure criterion follows the Mohr–Coulomb criterion as follows:

$$\sigma_1 = \sigma_3 \cot^2\left(\frac{\pi}{4} - \frac{\phi_0}{2}\right) + 2C_0 \cot\left(\frac{\pi}{4} - \frac{\phi_0}{2}\right) \quad (\beta_2 \le \beta_0 \text{ or } \beta_0 \le \beta_1) \tag{13}$$

where σ_1 is the maximum principal stress in MPa; σ_3 is the minimum principal stress in MPa; C_0 is the rock cohesion in MPa; C_w is the weak plane cohesion in MPa; ϕ_0 is the rock internal friction angle in degrees; ϕ_w is the weak plane friction angle in degrees; β_0 (given in degrees) is the angle between the normal direction of the weak surface and the maximum principal stress.

As an example, the distributions of effective radial stress and effective circumferential stress around the horizontal section of the Longmaxi Formation during the drilling and completion were evaluated and analyzed by using the test results of the in-situ stress in Well 1 of the Longmaxi shale formation. The basic data of Well 1 are shown below. The simulated wellbore trajectory is along the direction of the minimum horizontal principal stress and the well depth was 3800 m. The overlying strata pressure of ground stress was 92 MPa, the maximum horizontal principal stress was 97 MPa, and the minimum horizontal principal stress was 78.2 MPa. The pore pressure in the far field of Longmaxi Formation is 59.6 MPa, the drilling bottom liquid column pressure of the loading condition inside the borehole is 63.4 MPa, and the bottom hole flow pressure of test production is 39.22 MPa.

Fig. 13 and Fig. 14 compare and analyze the distribution of the effective radial stress and effective circumferential stress field in the horizontal section of the shale reservoir of the Longmaxi Formation in the drilling, fracturing, and completion processes.

Figs. 13 and 14 show that the wellbore formation's fluid–solid coupling effect has a significant impact on the effective stress field around the well, and there is a difference in the increase in the amplitude of the pore pressure near the borehole during the drilling, fracturing, and completion processes. The pore pressure increase amplitude of fracturing is larger than that for conventional drilling, and the pore pressure increase amplitude of conventional drilling is larger than that of the completion production. In conventional overbalanced drilling, the wellbore fluid migrates to the formation, which leads to a rise in the formation pore pressure and a decrease in the effective radial stress and tangential stress; it also increases the shear failure force. In the process of well completion and production, the formation fluid flows into the wellbore, which results in a decrease in the pore pressure around the

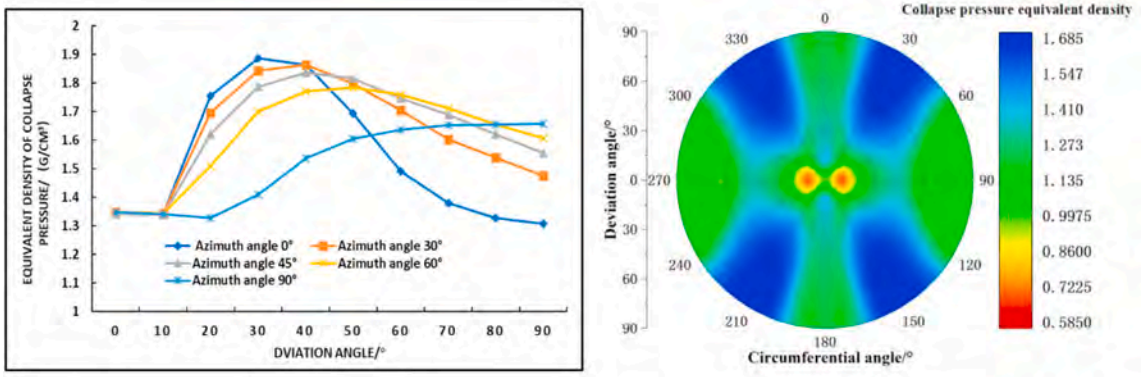

(a) Influence of azimuth angle on wellbore stability during the drilling process (b) Evaluation of borehole stability during drilling process

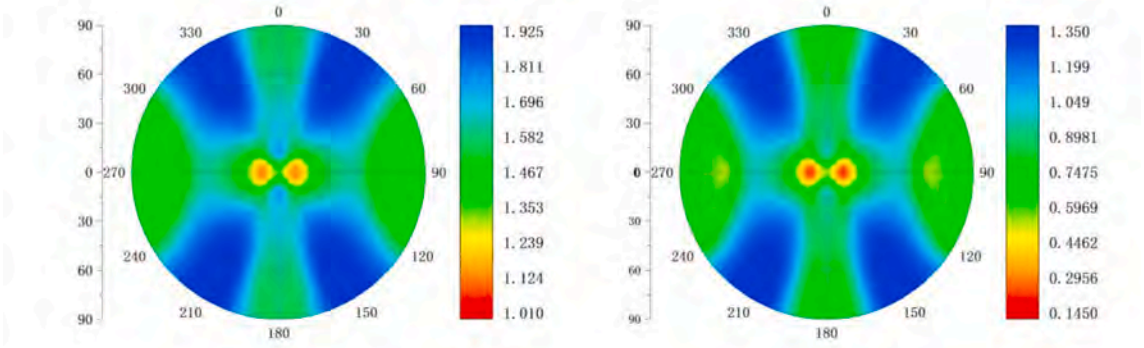

(c) Evaluation of borehole stability during the fracturing reformation process (d) Evaluation of borehole stability during completion and production process

Fig. 15. Wellbore stability comparison of Well 1 during the drilling and completion processes in the Longmaxi Formation.

well and an increase in the effective radial stress and tangential stress; it also decreases the shear failure.

At the same time, the dynamic changes in wellbore stability during drilling, fracturing, and completion of the Longmaxi shale reservoirs were evaluated and analyzed, as shown in Fig. 15.

Fig. 15 shows that the inclination angle and azimuth angle have obvious effects on the wellbore stability during the drilling process. As the inclination angle increases, the equivalent density of the formation collapse pressure first increases and then decreasing. The collapse pressure of the horizontal well drilled along the direction of the minimum horizontal principal stress is higher than the direction of the maximum horizontal principal stress.

There are differences in the borehole stability of the horizontal shale wells in the Longmaxi Formation under different working conditions. The main reason is the coupling effect of the seepage between the wellbore and the formation. In the process of fracturing, the effective liquid column pressure at the bottom of the well is the largest, which leads to an increase in the pore pressure near the borehole wall. This increase, in turn, leads to an increase in the borehole wall collapse pressure, and the equivalent density of the collapse pressure rises to 1.93 g/cm^3. The collapse pressure equivalent density during the drilling process was 1.69 g/cm^3. During the completion process, the formation fluid is poured back into the wellbore, which reduces the pore pressure near the wellbore and the equivalent density of the collapse pressure to 1.35 g/cm^3. The rate of pressure reduction is related to the wellbore permeability. During the completion and production process, the high collapse pressure area of the horizontal section is shaped like "four ears." The collapse pressure equivalent density is approximately 1.35 g/cm^3, and the collapse range angle is approximately 30°. This shows that the open hole completion of the horizontal wells in the Longmaxi Formation is still in the safe range, which shows that the open hole completion can be considered in this area. The pressure gradient of the bottomhole flow in the completion production should be controlled at 1.35 MPa/m.

5. Conclusions

(1) The content of brittle minerals, such as quartz and calcite in the shale reservoir of Longmaxi Formation is high, and the brittleness index is approximately 50%. The clay minerals are mainly illite, chlorite, and other weakly expansive clays.

(2) The shale of the Longmaxi Formation is dense with low porosity and permeability parameters, and the permeability is usually 10^{-2}–10^{-4} mD. The permeability of the rock sample with bedding cracks is relatively high, and the permeability along the direction of the bedding cracks is higher than the permeability perpendicular to the direction of the bedding cracks.

(3) Under different working fluids (oil-based drilling fluid, fracturing fluid, and completion fluid), the shale expansion performance of the Longmaxi Formation is very low, and the hydration expansion

strain is generally less than 0.1%; this proves that the hydration expansion ability of the shale in the Longmaxi Formation is weak.

(4) The shale rock strength of the Longmaxi Formation is high, but the anisotropic characteristics of mechanical strength are obvious. The compressive strength of the rock under downhole pressure is 150–304 MPa. The mechanical strength of the rock samples with the bedding cracks is low, and the compressive strength is within the range of 40–140 MPa. The immersion effect of the different working fluids has little influence on the mechanical properties of shale.

(5) Under different working conditions (drilling, fracturing, and completion production), there were differences in the laws of seepage migration between the wellbore and formation and the dynamic changes in the borehole pore pressure. Under drilling conditions, the equivalent density of formation collapse pressure was 1.69 g/cm^3, and the collapse pressure of the horizontal wells drilled along the minimum horizontal principal stress was higher than the collapse pressure in the direction of the maximum horizontal principal stress. During the fracturing process, the pore pressure near the borehole wall increases greatly, and the equivalent density of the collapse pressure increases to 1.93 g/cm^3. During the completion process, the borehole pore pressure was relieved, the borehole wall collapse pressure was reduced, and the collapse pressure equivalent density was reduced to approximately 1.35 g/cm^3. Open hole completion could be attempted in the horizontal section. We recommended that the pressure gradient of the bottomhole flow in the completion production be controlled at 1.35 MPa/m.

Credit author statement

Liu Houbin: Writing- Reviewing and Editing. Cui Shuai: Conceptualization, Methodology, Software, Meng Yingfeng: Supervision. Li Ze: Writing – original draft preparation. Yu Xingchuan: Visualization, Investigation. Sun Hangrui: Software, Validation. Zhou Yanxing: Data curation, Luo Yi: Data curation.

Declaration of competing interest

The authors declare that they have no known competing financial interests or personal relationships that could have appeared to influence the work reported in this paper.

References

An, M., Zhang, F., Elsworth, D., et al., 2020. Friction of Longmaxi shale gouges and implications for seismicity during hydraulic fracturing. J. Geophys. Res. Solid Earth 125 (8).

Barati, P., Keshtkar, S., Aghajafari, A., et al., 2016. Inhibition performance and mechanism of horsetail extract as shale stabilizer. Petrol. Explor. Dev. 43 (3), 522–527.

Chen, J., Zhou, Y., Zhu, K., et al., 2018. The analyses on wellbore stability in hard brittle shale in Dongying Formation of Jidong Oilfield. Sci. Technol. Eng. 18 (20), 109–115.

Chen, M., 2008. Rock Mechanics in Petroleum Engineering. Science Press, Beijing.

Chen, Z., Deng, J., Wei, B., et al., 2019. Borehole stability analysis of hard brittle shale based on damage theory. Sci. Technol. Eng. 19 (16), 87–94.

Ding, Y., Luo, P., Liu, X., Liang, L., 2018. Wellbore stability model for horizontal wells in shale formations with multiple planes of weakness. J. Nat. Gas Sci. Eng. 52, 334–347.

Fan, B., Tan, Q., Wei, B., et al., 2013. Feasibility mechanics analysis of open hole completion in Archean strata of Liaodong Bay. Sci. Technol. Eng. 9, 2474–2477.

Jaeger, J., Cook, N., 1979. Fundamentals of rock mechanics. Sci. Paperbaks 9 (2), 251–252.

Jin, Y., Chen, M., 2012. Wellbore Stability Mechanics. Science Press, Beijing.

Kanfar, M.F., Chen, Z., Rahman, S.S., 2017. Analyzing wellbore stability in chemically active anisotropic formations under thermal, hydraulic, mechanical and chemical loadings. J. Nat. Gas Sci. Eng. 41, 93–111.

Liang, L., Ding, Y., Liu, X., et al., 2016. Seepage-mechanochemistry coupling of wellbore stability in hard-brittle shale. Special Oil Gas Reservoirs 23 (2), 140–143 + 158.

Ma, T., Chen, P., 2015. A wellbore stability analysis model with chemical-mechanical coupling for shale gas reservoirs. J. Nat. Gas Sci. Eng. 26, 72–98.

Ma, T., Chen, P., Wang, X., et al., 2016. Numerical analysis method of pore pressure propagation around the borehole for shale gas reservoirs. Acta Pet. Sin. 37 (5), 660–671.

Ran, X., Wang, Y., Jia, S., 2015. Numerical simulation coupled with multi-fields on wellbore stability of shale. Chin. J. Undergr. Space Eng. 11 (S 2), 474–478.

Rick, R., Michael, J., James, E., et al., 2008. A practical use of shale petrophysics for stimulation design optimization: all shale plays are not clones of the Barnett Shale. SPE Annual Technical Conference and Exhibition.

Wang, P., Deng, J., Bai, Y., et al., 2018. Effect of drilling fluid soaking on the shale collapse pressure in Yanchang Formation. Special Oil Gas Reservoirs 25 (2), 159–163.

Wen, H., Chen, M., Jin, Y., et al., 2014. A chemo-mechanical coupling model of deviated borehole stability in hard brittle shale. Petrol. Explor. Dev. 41 (6), 817–823.

Wu, R., Kresse, O., Weng, X., et al., 2012. Modeling of Interaction of Hydraulic Fractures in Complex Fracture Networks. SPE-152052-MS.

Zhao, K., Fan, Y., Yu, B., et al., 2016. Research progress of wellbore stability in hard brittle shale. Oil Drill. Product. Technol. 38 (3), 277–285.